UDC 544.77, 665.642

DOI: 10.15372/CSD2021345

Cracking of Petroleum Vacuum Residues in the Presence of Hematite Nanoparticles

M. A. KOPYTOV[1], A. YU. GODYMCHUK[2], I. N. LAPIN[3], V. A. SVETLICHNYI[3]

[1]*Institute of Petroleum Chemistry, Siberian Branch of the Russian Academy of Sciences, Tomsk, Russia*

E-mail: kma@ipc.tsc.ru

[2]*Tobolsk Complex Scientific Station, Ural Branch of the Russian Academy of Sciences, Tobolsk, Russia*

[3]*National Research Tomsk State University, Tomsk, Russia*

(Received December 23, 2020; revised April 22, 2021)

Abstract

Hematite nanoparticles (23–150 nm) were obtained and dispersed in a hydrocarbon medium. The introduction of hematite nanoparticles at a concentration of 0.02 to 0.30 mass % into the oil residue during thermolysis allows increasing the yield of gasoline and reducing the yield of resins. The role of hematite is explained by its ability to selectively sorb resins and asphaltenes on its surface.

Keywords: hematite, magnetite, hematite nanoparticles, hematite nanoparticles in hydrocarbon medium, oil residues, cracking products

INTRODUCTION

Depletion of the resources of light and medium-weight oils leads to the necessity to enhance the extent of processing heavy hydrocarbon raw material and oil residues [1, 2]. Some publications [3–6] deal with the development of catalytic systems for this kind of processing. However, modern catalytic processes are ineffective for processing heavy hydrocarbon raw material with a high content of resinous and asphaltene components [1, 7]. It is generally accepted that if the Conradson coking index of the raw material exceeds 4 %, the use of the traditional catalytic cracking is unreasonable because of rapid failure of expensive catalysts [7, 8].

Investigations aimed at the use of nanosized particles for processing hydrocarbon raw material have been carried out for several recent years [3, 9–14]. The activity of iron-containing particles as initiating and catalyzing additives attracts attention first of all because these particles are readily available, cheap and ecologically friendly [4, 15–19].

Various methods are used to obtain iron oxide nanoparticles (NP): co-precipitation [20], sol-gel synthesis [21], microemulsion method [22], pyrolysis through spraying in the flame [23], decomposition of organic precursors [24], etc.

It has been demonstrated by the example of nickel oxide and iron oxide that the catalytic and adsorption activity of NP may depend on particle size [25]. The authors explain this effect not only by the change of the specific surface of NP with different sizes but also by a substantial change in the topology and functionality of the surface, which affects the reactivity of the particles [26].

The use of NP is very promising in different areas, but the application of some of them may be limited due to the tendency of NP to form aggregates and due to the fact that it is difficult to achieve their uniform distribution over the medium [27, 28]. To enhance the efficiency of their use as initiating additive in oil residue cracking, the method of particle dispersing in hydrocarbon medium was proposed in the work. In spite of the use of NP in thermal processing of heavy hydrocarbon raw material [9–14], in fact, any data on their efficient dispersing in the raw material are absent from the literature.

The goal of our work was to study the effect of the presence of dispersed and non-dispersed hematite (α-Fe_2O_3) particles on the composition of the products formed during the cracking of petroleum vacuum residues.

EXPERIMENTAL

The object of investigation

The initial raw material was the petroleum residue obtained through atmospheric-vacuum rectification of petroleum from West Siberia. The characteristics of the petroleum residue are presented in Table 1.

Preparation of catalytic dispersion

We studied NP of iron oxide (α-Fe_2O_3, hematite) obtained by annealing Fe_3O_4 nanopowder (magnetite). Magnetite was synthesized with the help of focused radiation of an Nd:YAG laser LS-2131M-20 (LOTIS TII, Belarus) at the wavelength of 1064 nm. Pulse duration was 7 ns, pulse repetition frequency was maintained at a level of 20 Hz. In this work, we used the full energy of the laser pulse of the nanosecond laser (150 mJ). Variation of focusing allows us to vary the laser power density on the surface of the target. In the case under consideration, we chose the power density of 400 MW/cm^2. An iron target (99.5 mass %) 40 × 40 × 5 mm in size was fixed in the cap at the back end of a cylindrical reactor made of quartz glass [29].

Magnetite powder was annealed in a SNOL 6.7/1300 muffle furnace (Latvia) at 500 °C in the air; the heating rate was 10 °C/min. After the required temperature was reached, the sample was kept for 4 h, and then cooled to room temperature [29].

The obtained sample of α-Fe_2O_3 NP was mixed with sodium oleate ($NaC_{18}H_{33}O_2$, 15 % solution in oleinic acid ($C_{17}H_{33}COOH$), IKO-Khim, Russia) in the industrial oil of I-8A grade (GOST 20799–88) at a mass ratio $Fe_2O_3/NaC_{18}H_{33}O_2$/oil equal to 1 : 2.2 : 16.8. Suspensions were prepared in two stages. At first, α-Fe_2O_3 NP and sodium oleate were mixed in a plastic vessel at a temperature of 25±2 °C with the help of ultrasonic treatment for 5 min, then oil was added into the resulting mixture, and subsequent treatment for 10 min at 50 °C was carried out. Samples were treated in a GRAD 28-35 ultrasonic bath (Grade Technology, Russia) at the power of 55 W.

The obtained suspension was introduced into oil residue to vary the total NP content in initial heavy oil from 0.02 to 0.30 mass %.

Investigation of nanoparticles

The phase composition of initial NP and samples after thermolysis was determined by means of X-ray diffraction (XRD). Diffraction patterns were recorded with a Discover D8 X-ray diffractometer (Bruker, Germany) with monochromatic CuK_α-radiation. Scanning was carried out within angle range $2\theta = 10–90°$. Results were processed

TABLE 1

Physicochemical characteristics of petroleum residue with a boiling point above 360 °C

Parameter	Value
Conventional viscosity, at a temperature of, °C:	
50	No free discharge
80	7.69
100	3.73
Mass concentration of mechanical impurities, %	0.01
Coking ability, mass %	6.57
Chilling temperature, °C	24
Flash point in a closed crucible, °C	203
Ash content, mass %	0.013
Density at 20 °C, kg/m^3	939.4
Component composition, mass %:	
Oils	85.7
Silica gel resins	12.4
Asphaltenes	1.9
Elemental composition, mass %:	
C	85.05
H	11.75
S	1.57
N	0.38
O	1.25
H/C ratio	1.65

using the database of diffraction spectra PDF-2 2010.

TEM images of the samples were taken with the help of the transmission electron microscope JEM-1400 (JEOL, Japan, resolution 0.24 nm); the maximal accelerating voltage was 200 kV.

The specific BET surface area of the powders was measured with a gas adsorption analyzer of specific surface and porosity TriStar II 3020 (Micromeritics, USA). Before analysis, the powder samples of the material were degassed in vacuum (10^{-2} Torr) at 200 °C for 2 h.

The distribution of hematite particles in suspension after dispersing was determined by means of the dynamic light scattering using the laser particle size analyzer Zetasizer Nano (Malvern, USA) at 25 °C (helium-neon laser, laser power 4 mW, wavelength 633 nm).

Cracking

Thermal cracking (thermolysis) of oil residue was carried out without the addition of preliminarily dispersed hematite particles (DP) and with the addition of dry non-dispersed (NDP) hematite particles. It was demonstrated in previous works [30, 31] by the example of oil residues of heavy oils that the introduction of hematite into oil residues in the amount of less than 1.00 mass % did not lead to a noticeable change in the composition of thermolysis products. For this reason, we chose this concentration (1.00 mass %) of hematite NDP for comparison.

After the introduction of NP into heavy oil residue, the mixture was homogenized at 70 °C for 15 min by mechanical mixing and kept at this temperature for 15 min in an ultrasonic bath at a power of 55 W.

To evaluate the effect of sodium oleate, oleinic acid and the addition of industrial oil on the process of heavy oil residue cracking, in one of the experiments, we used a mixture of sodium oleate in oleinic acid/industrial oil at a ratio of 2.2 : 16.8 in the amount of 5.70 mass %. This sample is marked "without hematite" in the Figures.

After the preparation of the reaction mixture, the samples were charged in the amount of 7.0 g into an autoclave 10 cm^3 in volume. After assembling, the autoclave was blown with nitrogen through the gas outlet valve to provide an inert medium.

Thermal cracking of the samples was carried out at 435 °C for 90 min. Then the autoclave was cooled to room temperature, gas products were sampled, and then liquid and solid products of cracking were taken out. The choice of the conditions and the procedure of thermolysis was based on the results of our previous investigations [30–32].

Investigation of initial petroleum residue and the products of thermal cracking

Gaseous products were analyzed with the help of Kristall-5000 chromatograph (Khromatek, Russia) according to GOST 31371.3–2008.

The hydrocarbon composition of gasoline fractions was determined by means of gas chromatography according to GOST R 52714–2018 with the Kristall-5000 chromatograph (capillary column DB-1 (Agilent, USA) with the inner diameter 0.25 mm, 100 m long, nonpolar, 100 % dimethylpolysiloxane).

Due to the small amount of the formed thermolysis products, the content of light fractions in them was estimated from the data of thermogravimetric analysis similarly to the procedure described in [33]. Thermogravimetric analysis was carried out with a Q-1000 derivatograph (MOM, Hungary). The loss of sample mass was recorded within the temperature range 50 to 360 °C with a heating rate 10 °C/min.

The content of resins and asphaltenes in oil residue and the products of cracking was analyzed using a standard procedure similar to that described in our previous works [30–32]. Asphaltenes were isolated by diluting the sample with *n*-hexane in the volume ratio of 1 : 40. After dilution, the resulting solution was kept for 1 day in the dark; the formed precipitate was separated by filtering. The precipitate was placed in a paper cartridge and washed with *n*-hexane in the Soxhlet apparatus to remove oils and resins (maltenes), then asphaltenes were washed off the paper cartridge with chloroform, the solvent was distilled, and the asphaltenes were dried to a constant mass.

After solvent distillation from the united hexane solution (after asphaltene precipitation and washing), maltenes were obtained. They were deposited on a layer of activated silica gel ASK (at a ratio of 1 : 15), the resulting mixture of silica gel with adsorbed material was loaded into Soxhlet apparatus, and oils were washed off sequentially with *n*-hexane, and then resins were washed off with a mixture of ethanol and benzene (1 : 1) at the boiling points of these solvents. After solvent removal, the contents of oils and resins in the sample were determined.

Analysis of the content of carbon, hydrogen, nitrogen, and oxygen was carried out with the help of an elemental analyzer Vario EL Cube (Elementar, Germany). Sulphur content was determined by burning and subsequent absorption of the formed sulphur oxides by sodium carbonate solution and titration with hydrochloric acid [34].

RESULTS AND DISCUSSION

Characteristics of nanoparticles

The phase composition of NP under study included mainly hematite phase (α-Fe_2O_3), the specific surface area was 19.2 m^2/g [29].

According to the data of TEM analysis, the particle size distribution was 22–150 nm (Fig. 1). The data of the calculation of average particle size according to the BET procedure (59.6 nm) are in agreement with the data of electron microscopy (67 nm). The particles form aggregates with a size distribution from 125 to 447 nm (see Fig. 1), the shape of the particles is equiaxial. Analysis of TEM images allowed us to see that the particles are held together in agglomerates by the interparticle (coagulation, non-phase) interaction, therefore, chemical processes may take place over the whole surface of the used NP. When in hydrocarbon medium, NP form suspensions characterized by the unimodal size distribution within 220–712 nm, with the average aggregate size 414 nm.

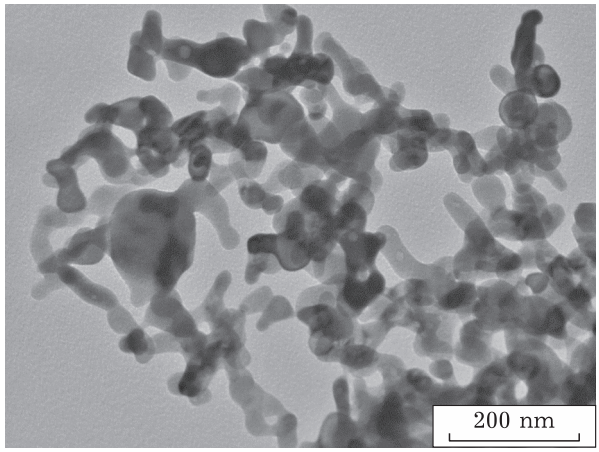

Fig. 1. TEM image of hematite (α-Fe_2O_3) nanoparticles.

Composition of the products of thermal cracking

The composition of the products of thermal cracking is presented in Fig. 2 and 3. The fractions of solid and gaseous components in thermolysis products obtained without hematite particles are 1.8 and 2.7 mass %, respectively. After the introduction of hematite NDP (as dry powder) in the amount of 1.00 mass %, the yield of gaseous products is 3.9 mass %, and the yield of solid products is 4.2 mass %. The introduction of hematite NP in the form of suspension prepared preliminarily leads to a substantial increase in the fraction of solid and gaseous products (see Fig. 2). In comparison with the products of cracking without the addition of hematite particles, the fraction of gaseous and solid components increases in the presence of hematite DP by a factor of 2.2 and 3.4, respectively, which is explained by more intense thermal destruction in the presence of these particles.

Preliminary NP dispersing allows an increase in the surface of hematite contact with the components of the raw material, and thus its availability increases. Finely dispersed particles may also promote dispersing of the phase of coke precursor and thus change the rate of the formation of solid products (coke), as shown in [35]. The stability of the dispersed system may be the reason of the nonlinear yield of solid products depending on the concentration of hematite introduced into the raw material in the form of particles.

The effect of hematite is also in the selective sorption of asphaltenes on its surface. It is demonstrated in [36–38] that asphaltenes are readily adsorbed on the oxides of transition metals, in particular iron oxides. A decrease in the concentration of asphaltenes in the products of thermolysis is likely to be explained by the selective sorption of resins and asphaltenes on the surface of hematite particles and the subsequent destruction of these compounds. The substance composition of the products of thermolysis is shown in Fig. 3.

The introduction of preliminarily dispersed hematite NP allows obtaining the products with lower resin content (see Fig. 3).

With an increase in the concentration of hematite DP from 0.02 to 0.30 mass %, the percentage of asphaltenes gradually increases from 1.7 to 2.5 mass %, and the yield of resins is within the range of 3.2 to 3.8 mass %, while the content of oils gradually decreases from 85.8 to 82.4 mass %. A decrease in the content of oils, together with a decrease in the fraction of resins, is explained by their involvement into the destruction process, which causes an increase in the yield of low-boiling fractions with initial boiling points below 200 °C (initial boiling points, i.b.p., Fig. 4) and an increase in the amount of solid and gaseous products (see Fig. 2).

According to the data on the fraction composition, the introduction of hematite DP leads to an increase in the yield of gasoline fractions (i.b.p. 200 °C) by 9.0–16.4 %, while the yield of diesel fractions decreases by 6.7–10.9 mass % (see Fig. 4). The ratio of the yields of diesel to gasoline fractions changes almost by a factor of 3, while the total yield of the fractions (i.b.p. 360 °C) changes only slightly.

The group composition of the fraction with i.b.p. 200 °C and gaseous products is presented in Table 2.

The introduction of dispersed and non-dispersed hematite NP leads to an increase in the fraction of isoalkanes, naphthenes and alkenes in

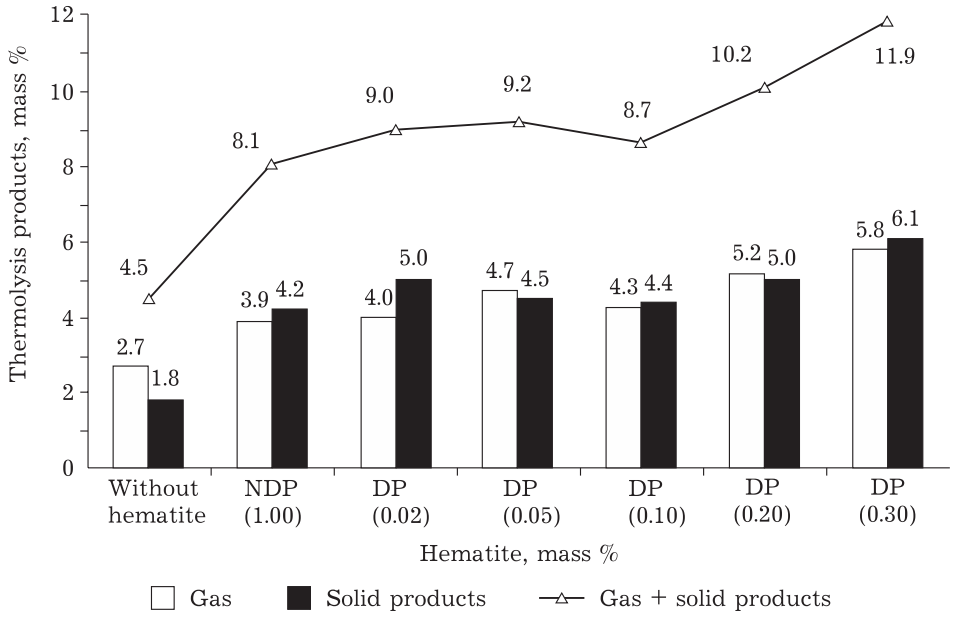

Fig. 2. The yield of solid and gaseous products of cracking with the addition of hematite nanoparticles into petroleum residue and without this additive. Here and in Fig. 3, 4: NDP, DP – non-dispersed and dispersed hematite particles, respectively; hematite content (mass %) is indicated in parentheses.

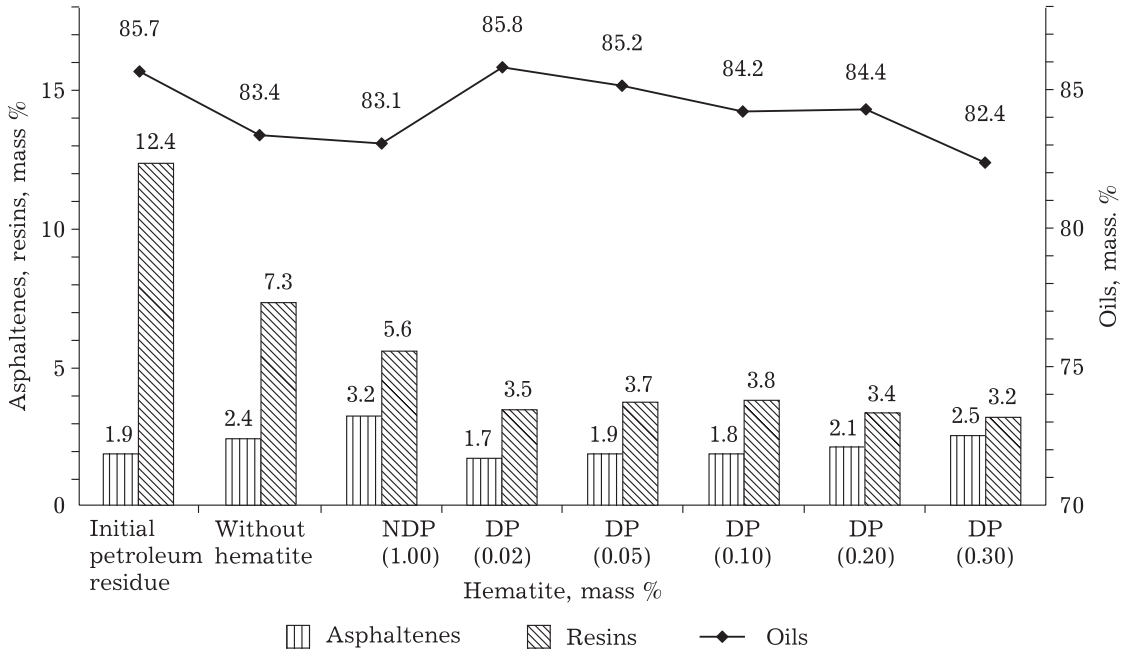

Fig. 3. The substance composition of the liquid products of cracking petroleum residue. For designations, see Fig. 2.

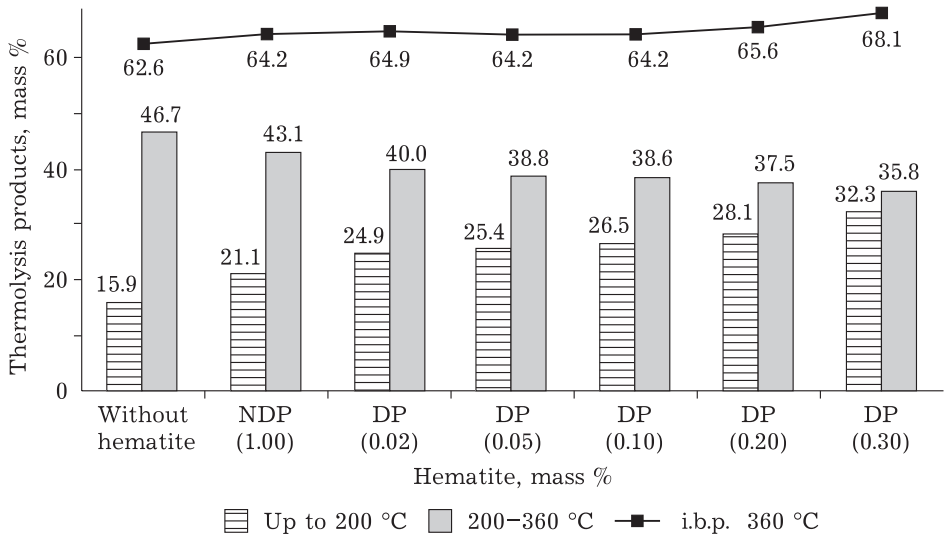

Fig. 4. Fractional composition of the products of cracking of petroleum residue. For designations, see Fig. 2; i.b.p. is the initial boiling point, °C.

TABLE 2

Composition of the fraction with i.b.p. 200 °C and gaseous products of cracking of petroleum residue, mass %

Components	Without additives	Content of hematite nanoparticles, mass %					
		Without dispersing	Dispersed preliminarily				
		1.00	0.02	0.05	0.10	0.20	0.30
Composition of the fraction with i.b.p. 200 °C							
n-Alkanes	5.4	4.0	6.3	6.8	8.0	7.5	5.5
Isoalkanes	4.1	7.5	7.8	7.2	7.7	8.3	11.5
Arenes	2.6	2.4	2.9	2.7	2.7	3.5	4.9
Naphthenes	1.9	3.4	4.3	5.0	4.2	4.7	5.2
Alkenes	1.4	3.3	3.1	3.1	3.3	3.9	4.2
Not determined	0.4	0.4	0.5	0.6	0.6	0.3	1.0
Total yield of gasoline fractions, mass %	15.9	21.1	24.9	25.4	26.5	28.1	32.3
Content of gaseous components							
H_2	0.001	< 0.001	0.009	0.013	0.013	0.012	0.015
CO	< 0.001	0.025	0.014	0.027	0.028	0.030	0.034
CO_2	0.027	0.047	0.023	0.046	0.050	0.080	0.121
CH_4	0.360	0.371	1.017	1.276	1.297	1.332	1.400
C_2H_4	0.021	0.019	0.014	0.021	0.023	0.023	0.062
C_2H_6	0.661	0.742	1.063	1.234	1.181	1.341	1.468
C_3H_8	0.828	1.216	1.086	1.272	1.099	1.405	1.676
C_3H_6	0.063	0.099	< 0.001	0.002	0.001	0.009	0.052
Alkanes C_4	0.483	0.790	0.533	0.612	0.486	0.663	0.694
Alkanes C_4	0.048	0.121	0.036	0.032	0.031	0.042	0.052
Alkanes C_5	0.208	0.468	0.205	0.183	0.124	0.213	0.222
Total yield of gaseous products, mass %	2.70	3.90	4.00	4.72	4.30	5.15	5.80

Note. i.b.p. is the initial boiling point, °C.

the gasoline fractions of thermolysis products. The concentrations of *n*-alkanes in the resulting fractions change non-linearly. An increase in the yield of aromatic hydrocarbons is explained by the destruction of resinous and asphaltenous components.

After the introduction of hematite, the yield of alkenes increases both in liquid products and in gases, which points to the possible destruction of hydrocarbon components.

After the introduction of dispersed and non-dispersed hematite NP, carbon monoxide (CO) appears in the gaseous products, and the fraction of carbon dioxide (CO_2) increases, which points to the oxidation-reduction processes. Hematite (α-Fe_2O_3) may be recovered in this process into magnetite (Fe_3O_4), which is accompanied by the partial oxidation of the components of raw material with the formation of CO and CO_2 [4, 16].

The X-ray diffraction patterns of the initial hematite powder which was used to prepare suspensions (sample *1*), coke-like cracking products obtained in the presence of 1.00 mass % of non-dispersed hematite NP (sample *2*) and in the presence of 0.3 mass % of dispersed hematite NP (sample *3*) are shown in Fig. 5.

The diffraction pattern of sample *1* contains only characteristic reflections characteristic of hematite (see Fig. 5). Reflections characteristic of hematite are absent from the diffraction patterns of samples *2* and *3*, but some peaks appear that may point to the formation of magnetite or maghemite. An intense reflection at 26.5° (see Fig. 5) is characteristic of carbon. It is better pronounced for sample *3* because the content of iron oxides in this coke-like product is three or even more times lower than that in sample *2*.

CONCLUSION

It is demonstrated that the presence of nanosized hematite particles during thermolysis leads to a change in the direction of thermal transformations of the components of heavy petroleum raw material.

The introduction of dispersed nanosized hematite particles allows an increase in the yield of gasoline fractions and a decrease in the yield of resins.

In the presence of hematite, the composition of gaseous products also changes significantly: carbon monoxide appears, and the fraction of carbon dioxide increases, which points to the oxidation-reduction processes. Hematite (α-Fe_2O_3) may be reduced in this process to form magnetite (Fe_3O_4).

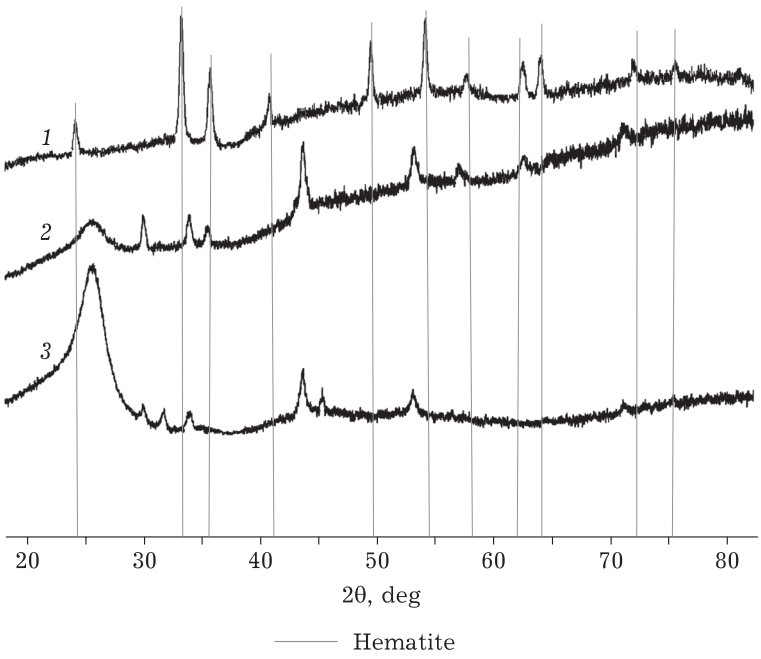

Fig. 5. X-ray diffraction patterns of samples: *1* – initial hematite powder used to prepare suspensions; *2* – coke-like products of cracking, obtained in the presence of 1.00 mass % non-dispersed hematite nanoparticles (as the dry powder); *3* – coke-like products of cracking, obtained in the presence of 0.30 mass % dispersed hematite nanoparticles (introduced in the form of suspension).

Acknowledgements

The work was carried out within the State Assignment to the IPC SB RAS (Tomsk), financed by the Ministry of Science and Higher Education of the Russian Federation.

REFERENCES

1 Castaceda L. C., Mucoz J. A. D., Ancheyta J., Current situation of emerging technologies for upgrading of heavy oils, *Catal. Today*, 2014, Vol. 220–222, P. 248–273.
2 Castaceda L. C., Mucoz J. A. D., Ancheyta J., Combined process schemes for upgrading of heavy petroleum, *Fuel*, 2012, Vol. 100, P. 110–127.
3 Muraza O., Hydrous pyrolysis of heavy oil using solid acid minerals for viscosity reduction, *J. Anal. Appl. Pyrolysis*, 2015, Vol. 114, P. 1–10.
4 Wang D., Jin L., Li Y., Hu H., Partial oxidation of vacuum residue over Al and Zr-doped α-Fe_2O_3 catalysts, *Fuel*, 2017, Vol. 210, P. 803–810.
5 Iskandar F., Dwinanto E., Abdullah M., Muraza O., Viscosity reduction of heavy oil using nanocatalyst in aquathermolysis reaction, *KONA Powder and Particle Journal*, 2016, Vol. 33, P. 3–16.
6 Eshraghian A., Husein M. M., Catalytic thermal cracking of Athabasca VR in a closed reactor system, *Fuel*, 2018, Vol. 217, P. 409–419.
7 Khadzhiev S. N., Gerzeliev I. M., Kapustin V. M., Kadiev Kh. M., Demenyev K. I., Pakhmanova O. A., Catalytic cracking in today's deep-conversion refinery, *Petroleum Chemistry*, 2011, Vol. 51, No. 1, P. 32–38.
8 Al-Sabawi M., Chen J., Ng S., Fluid catalytic cracking of biomass-derived oils and their blends with petroleum feedstocks: A review, *Energy & Fuels*, 2012, Vol. 26, No. 9, P. 5355–5372.
9 Muraza O., Galadima A., Aquathermolysis of heavy oil: A review and perspective on catalyst development, *Fuel*, 2015, Vol. 157, P. 219–231.
10 Kim S. H., Kim K. D., Lee D., Lee Y. K., Structure and activity of dispersed Co, Ni, or Mo sulfides for slurry phase hydrocracking of vacuum residue, *J. Catal.*, 2018, Vol. 364, P. 131–140.
11 Al-Marshed A., Hart A., Leeke G., Greaves M., Wood J., Effectiveness of different transition metal dispersed catalysts for *in situ* heavy oil upgrading, *Ind. Eng. Chem. Res.*, 2015, Vol. 54, No. 43, P. 10645–10655.
12 Ahn H. K., Park S. H., Sattar S., Woo S. I., Vacuum residue upgrading through hydroprocessing with subcritical water, *Catal. Today*, 2016, Vol. 265, P. 118–123.
13 Hosseinpour M., Akizuki M., Oshima Y., Soltani M., Influence of formic acid and iron oxide nanoparticles on active hydrogenation of PAHs by hot compressed water. Isotope tracing study, *Fuel*, 2019, Vol. 254, Art. 115675.
14 Hashemi R., Nassar N. N., Pereira-Almao P., Nanoparticle technology for heavy oil in situ upgrading and recovery enhancement: Opportunities and challenges, *Applied Energy*, 2014, Vol. 133, P. 374–387.
15 Sun Z. Q., Ma F. Y., Liu X. J., Wu H. H., Niu C. G., Su X. T., Liu J. M., Large-scale synthesis and catalysis of oleic acid-coated Fe_2O_3 for co-liquefaction of coal and petroleum vacuum residues, *Fuel Process. Technol.*, 2015, Vol. 139, P. 173–177.
16 Hosseinpour M., Fatemi S., Ahmadi S. J., Catalytic cracking of petroleum vacuum residue in supercritical water media: Impact of α-Fe_2O_3 in the form of free nanoparticles and silica-supported granules, *Fuel*, 2015, Vol. 159, P. 538–549.
17 Wang D., Jin L., Li Y., Wei B., Yao D., Hu H., Upgrading of vacuum residue with chemical looping partial oxidation over Fe-Mn mixed metal oxides, *Fuel*, 2019, Vol. 239, P. 764–773.
18 Abu Tarboush B. J., Husein M. M., Dispersed Fe_2O_3 nanoparticles preparation in heavy oil and their uptake of asphaltenes, *Fuel Process. Technol.*, 2015, Vol. 133, P. 120–127.
19 Wang D., Jin L., Li Y., Yao D., Wang J., Hu H., Upgrading of vacuum residue with chemical looping partial oxidation over Ce doped Fe_2O_3, *Energy*, 2018, Vol. 162, P. 542–553.
20 Lee S. J., Jeong J. R., Shin S. C., Kim J. C., Kim J. D., Synthesis and characterization of superparamagnetic maghemite nanoparticles prepared by coprecipitation technique, *J. Magn. Magn. Mater.*, 2004, Vol. 282, P. 147–150.
21 Da Costa G. M., De Grave E., De Bakker P. M. A., Vandenberghe R. E., Synthesis and characterization of some iron oxides by sol-gel method, *J. Solid State Chem.*, 1994, Vol. 113, No. 2, P. 405–412.
22 Chin A. B., Yaacob I. I., Synthesis and characterization of magnetic iron oxide nanoparticles via w/o microemulsion and massart's procedure, *J. Mater Process. Technol.*, 2007, Vol. 191, No. 1–3, P. 235–237.
23 Strobel R., Pratsinis S. E., Direct synthesis of maghemite, magnetite and wustite nanoparticles by flame spray pyrolysis, *Advanced Powder Technology*, 2009, Vol. 20, No. 2, P. 190–194.
24 Galukhin A. V., Erokhin A. A., Osin Y. N., Nurgaliev D. K., Catalytic aquathermolysis of heavy oil with iron tris(acetylacetonate): Changes of heavy oil composition and in situ formation of magnetic nanoparticles, *Energy & Fuels*, 2015, Vol. 29, No. 8, P. 4768–4773.
25 Marei N. N., Nassar N. N., Vitale G., Hassan A., Zurita M. J. P., Effects of the size of NiO nanoparticles on the catalytic oxidation of Quinolin-65 as an asphaltene model compound, *Fuel*, 2017, Vol. 207, P. 423–437.
26 Marei N. N., Nassar N. N., Vitale G., The effect of the nanosize on surface properties of NiO nanoparticles for the adsorption of Quinolin-65, *Phys. Chem. Chem. Phys.*, 2016, Vol. 18, No. 9, P. 6839–6849.
27 Ma J., Jing Y., Gao L., Chen J., Wang Z., Weng L., Li H., Chen Y., Li Y., Hetero-aggregation of goethite and ferrihydrite nanoparticles controlled by goethite nanoparticles with elongated morphology, *Sci. Total Environ.*, 2020, Vol. 748, Art. 141536.
28 Shrestha S., Wang B., Dutta P., Nanoparticle processing: Understanding and controlling aggregation, *Adv. Colloid Interface Sci.*, 2020, Vol. 27, Art. 102162.
29 Svetlichnyi V. A., Shabalina A. V., Lapin I. N., Goncharova D. A., Velikanov D. A., Sokolov A. E., Study of iron oxide magnetic nanoparticles obtained *via* pulsed laser ablation of iron in air, Appl. Surf. Sci., 2018, Vol. 462, P. 226–236.
30 Golovko A. K., Kopytov M. A., Sharonova O. M., Kirik N. P., Anshits A. G., Cracking of heavy oils using catalytic additives based on coal fly ash ferrospheres, *Catal. Ind.*, 2015, Vol. 7, No. 4, P. 293–300.
31 Kopytov M. A., Golovko A. K., Kirik N. P., Anshits A. G., Thermal transformations of high-molecular-mass-components of heavy petroleum residues, *Petroleum Chemistry*, 2013, Vol. 53, No. 1, P. 14–19.
32 Kopytov M. A., Boyar S. V., Mozhaiskaya M. V., Thermal transformations of petroleum residue components in the presence of power-plant flyash ferrospheres and sunflower oil, *Petroleum Chemistry*, 2020, Vol. 60, No. 3, P. 348–357.
33 Ortiz-Moreno H., Ramírez J., Cuevas R., Marroquín G., Ancheyta J., Heavy oil upgrading at moderate pressure using dispersed catalysts: Effects of temperature, pressure

and catalytic precursor, *Fuel*, 2012, Vol. 100, P. 186–192.
34 Klimova V. A., Basic Micromethods for the Analysis of Organic Compounds, Moscow, Khimiya, 1975. (In Russ.).
35 Tanabe K., Gray M. R., Role of fine solids in the coking of vacuum residues, *Energy & Fuels*, 1997, Vol. 11, No. 5, P. 1040–1043.
36 Nassar N. N., Hassan A., Pereira-Almao P., Comparative oxidation of adsorbed asphaltenes onto transition metal oxide nanoparticles, *Colloids and Surfaces A: Physicochem. Eng. Aspects*, 2011, Vol. 384, No. 1–3, P. 145–149.
37 Hosseinpour N., Mortazavi Y., Bahramian A., Khodatars L., Khodadadi A. A. Enhanced pyrolysis and oxidation of asphaltenes adsorbed onto transition metal oxides nanoparticles towards advanced in situ combustion EOR processes by nanotechnology, *Appl. Catal. A: General*, 2014, Vol. 477, P. 159–171.
38 Setoodeh N., Darvishi P., Lashanizadegan A., A comparative study to evaluate the performance of coated Fe_3O_4 nanoparticles for adsorption of asphaltene from crude oil in bench scale, *J. Dispers. Sci. Technol.*, 2018, Vol. 39, No. 5, P. 711–720.